Acoustic metamaterial modeling using space-coiling resonators

Luciano S. Oliveira[1], Victor G. R. C. Dos Santos[1], Edson J. P. Miranda Jr.[1,2], José Maria C. Dos Santos[1]

[1]*Computational Mechanics Department, University of Campinas*
Rua Mendeleyev, 200, CEP 13083-970, Campinas, SP, Brazil
l261283@dac.unicamp.br, v228253@dac.unicamp.br, zema@unicamp.br
[2]*Federal Institute of Maranhão*
Rua Afonso Pena, 174, CEP 65010-030, São Luís, MA, Brazil
edson.jansen@ifma.edu.br

Abstract. In the last decades the development of metamaterial has motivated new solutions for noise control, where labyrinthine type absorbers emerged recently. Due to their attracting features, these types of absorbers have been investigated. The strategy is to bend and coil up quarter-wavelength sound damping tube. The original bulky volume is decreased into a subwavelength scale, and the absorber with a coiling chamber can produce a high sound absorption at low frequency. The aim of this paper is to establish reliable analytical and numerical approaches for the designing and modeling of an effective metamaterial with space-coiling resonators. A duct-resonator acoustic device is modeled by the Transfer Matrix (TM) and the Finite Element (FE). Simulated examples are performed and the compared between the methods. The duct-resonator efficiency to attenuate the sound is evaluated.

Keywords: Coiling space, acoustic metamaterial, transfer matrix method.

1 Introduction

Mufflers are important elements for noise reduction and control, reducing the sound transmitted along a duct [1]. However, the noise control at low frequencies is a challenge due to weak interaction with the structure in the case of long wavelength [2].

Helmholtz resonators (HR) are used effectively to attenuate noise in a narrow bandwidth around the resonant frequency [3], having several applications in churches, dampers in tubes and ducts, among other [4]. However, for low frequency noise, the use may be limited by volume restrictions [5], as the resonant frequency is governed by physical dimensions, neck, cavity or both [3]. Thus, it is important to decrease the resonance frequency without increasing the volume, or to reduce the volume without increasing the resonance frequency [5].

The use of space coiling resonators brings advantages in terms of dimensions. Shi and Mak [6] studied an HR resonator with a spiral neck and their results showed a resonant frequency of 48 Hz for a four-turn spiral. Wang et al. [2] studied a coiled partition resonator extending into a cavity and noted that by extending the partition the wavelength of the resonant frequency can be up to 26 times the cavity length.

One way to increase the attenuation range in a duct is to distribute the HR's periodically along the duct, generating prohibited frequency bands, or bandgaps, where harmonic waves do not propagate [7].

The objective of this work is to use the transfer matrix method (TM) to model the duct noise attenuation using coiled side branch HR arranged periodically. Equivalent Helmholtz resonator is modeled and a numerical validation is done using Comsol Multiphysics software by means of the finite element method (FE).

2 Transfer matrix modeling

The 2D model consists of a Helmholtz like side-branch resonator, which comprises a coiling neck partition inside a cavity connected to a main duct (Fig. 1a). The coiling neck dimensions are the width w_n and the midline

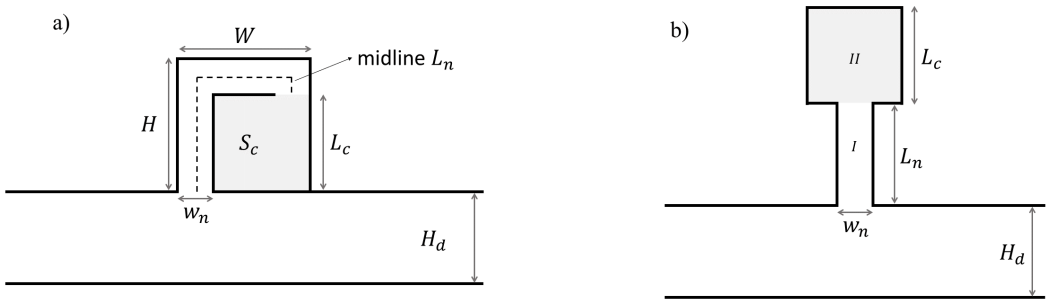

Figure 1. Model of coiling neck resonators: (a) coiling-HR and (b) equivalent-HR.

L_n, while the total cavity dimensions are height H and width W. The main duct dimensions are height H_d and cross-section area S_d. The coiling neck gradually extends into the cavity center and the remaining cavity of area S_c and side length L_c is created. When no coiling neck is included ($L_n = 0$) the side-branch resonator becomes an HR with cavity and small neck (main duct thickness). In the reverse way, when the coiling neck increases, the cavity area is reduced, and in the limit ($S_c = 0$) it becomes a coiling quarter wave length tube. An equivalent model proposed by [2] is shown in Fig. 1b, where the coiling neck is unwind and becomes a straight one, to obtain an equivalent HR with neck width w_n, neck length L_n, cavity area S_c and side length cavity L_c.

The formulation presented is based on [2, 8]. The (TM) method is applied to model the sound transmission in the equivalent model, which is divided in two partitions: (I) neck and (II) square cavity. For the partition I, the acoustic pressures (p_0 and p_l) and volume velocities (U_0 and U_l) at the neck input and output ends can be related as [8]:

$$\left\{ \begin{array}{c} p_{0_I} \\ U_{0_I} \end{array} \right\} = \left[\begin{array}{cc} cos(kL'_n) & j\frac{\rho c}{S_n}\sin(kL'_n) \\ j\frac{S_n}{\rho c}\sin(kL'_n) & cos(kL'_n) \end{array} \right] \left\{ \begin{array}{c} p_{l_I} \\ U_{l_I} \end{array} \right\}, \tag{1}$$

where S_n is the neck cross-sectional area, L'_n is the effective length of the neck (details in section 2.1), ρ and c are mass density and sound velocity of air, respectively. In order to account for the damping effect of air viscosity a complex wavenumber is included, $k = \hat{k}(1 + j\eta/2)$, where $\hat{k} = \omega/c$ is the wavenumber, η is the loss factor, ω is the circular frequency and c is air wave velocity.

For the partition II, the sound transmission between cavity entrance and bottom can be formulated as:

$$\left\{ \begin{array}{c} p_{0_{II}} \\ U_{0_{II}} \end{array} \right\} = \left[\begin{array}{cc} cos(kL_c) & j\frac{\rho c}{S_c}\sin(kL_c) \\ j\frac{S_c}{\rho c}\sin(kL_c) & cos(kL_c) \end{array} \right] \left\{ \begin{array}{c} p_{l_{II}} \\ U_{l_{II}} \end{array} \right\}, \tag{2}$$

where S_c and L_c are the cross-sectional area and length of the resonator cavity, respectively. By applying the sound pressure and volume velocity continuity at the coupling point between neck and cavity, the relation between acoustic pressures and volume velocities at the tube neck entrance and at the cavity bottom can be written as:

$$\left\{ \begin{array}{c} p_{0_I} \\ U_{0_I} \end{array} \right\} = \left[\begin{array}{cc} cos(kL'_n) & j\frac{\rho c}{S_n}\sin(kL'_n) \\ j\frac{S_n}{\rho c}\sin(kL'_n) & cos(kL'_n) \end{array} \right] \left[\begin{array}{cc} cos(kL_c) & j\frac{\rho c}{S_c}\sin(kL_c) \\ j\frac{S_c}{\rho c}\sin(kL_c) & cos(kL_c) \end{array} \right] \left\{ \begin{array}{c} p_{l_{II}} \\ U_{l_{II}} \end{array} \right\}. \tag{3}$$

Then, Eq. (3) can be rewritten in a compact form as:

$$\left\{ \begin{array}{c} p_{0_I} \\ U_{0_I} \end{array} \right\} = \mathbf{T}_1\mathbf{T}_2 \left\{ \begin{array}{c} p_{l_{II}} \\ U_{l_{II}} \end{array} \right\} = \left[\begin{array}{cc} A & B \\ C & D \end{array} \right] \left\{ \begin{array}{c} p_{l_{II}} \\ U_{l_{II}} \end{array} \right\}. \tag{4}$$

Considering that the cavity bottom is a rigid wall, thus there is no volume velocity and $U_{l_{II}} = 0$. By substituting in the Eq. (4) produces the HR acoustic impedance as:

$$Z_{HR} = \frac{p_{0_I}}{U_{0_I}} = \frac{A}{C}, \tag{5}$$

and the HR transfer matrix can be obtained as:

$$\mathbf{T}_{HR} = \begin{bmatrix} 1 & 0 \\ 1/Z_{HR} & 1 \end{bmatrix}. \tag{6}$$

2.1 HR neck end corrections

The correction factor at the HR neck ends must be added to its physical length to obtain the effective length ($L'_n = L_n + \delta_e + \delta_i$). A correction factor for the neck-cavity interface, proposed by [9], is given by:

$$\delta_e = 0.82r\left(1 - 1.33\frac{r}{R}\right), \tag{7}$$

where r and R are the HR neck and cavity radius.

Obtained by boundary element analysis the correction factor of neck-duct interface, proposed by [10], is given by:

$$\delta_i = r\left\{0.8216 - 0.0644\left(\frac{r}{a}\right) - 0.694\left(\frac{r}{a}\right)^2\right\};\ \frac{r}{a} \leq 0.4, \tag{8}$$

$$\delta_i = r\left\{0.9326 - 0.6196\left(\frac{r}{a}\right)\right\};\ \frac{r}{a} > 0.4, \tag{9}$$

where r and a is the HR neck and the coupled main duct radius.

3 Periodic HR modeling

By applying a similar relation as presented in the Eq. (1), the main duct transfer matrix can be obtained as [8]:

$$\mathbf{T}_d = \begin{bmatrix} cos(kL_d) & j\frac{\rho c}{S_d}sin(kL_d) \\ j\frac{S_d}{\rho c}sin(kL_d) & cos(kL_d) \end{bmatrix}, \tag{10}$$

where L_d is the length of the duct before and after the HR.

Figure 2 shows the HR layout periodically distributed along a duct. It can be seen that the unit-cell is a combination of three elements: one left-side duct, one HR, and one right-side duct.

From the Eqs. (6) and (10) the unit-cell transfer matrix for the periodic system can be obtained as:

$$\mathbf{T}_{cell} = \mathbf{T}_d\mathbf{T}_{HR}\mathbf{T}_d = \begin{bmatrix} A_c & B_c \\ C_c & D_c \end{bmatrix}. \tag{11}$$

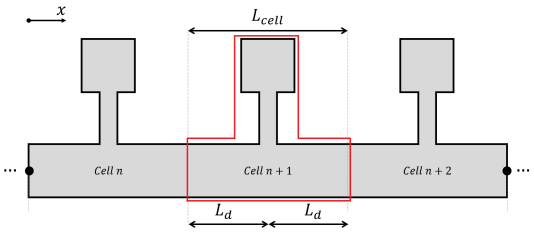

Figure 2. Periodic Helmholtz resonators emphasizing the duct-HR unit-cell (*red line*).

Thus, the acoustic pressure and volume velocity at the left-end side and right-end side of the periodic cell are given by:

$$\begin{bmatrix} p_0 \\ U_0 \end{bmatrix} = \mathbf{T}_{cell} \begin{bmatrix} p_l \\ U_l \end{bmatrix}, \tag{12}$$

Rewriting the Eq. (12) in compact form:

$$\mathbf{q}_l = \mathbf{T}_{cell}\mathbf{q}_r, \tag{13}$$

where $\mathbf{q}_r = \{p_l \; U_l\}^T$ and $\mathbf{q}_l = \{p_0 \; U_0\}^T$ are the state vectors of the right-end and left-end side of the unit cell, respectively.

Considering the consecutive unit cells n and $n+1$ (Fig. 2), and from the compatibility condition and continuity of volume velocity and acoustic pressure it has $\mathbf{q}_r^n = \mathbf{q}_l^{n+1}$. By replacing it in the Eq. 13 one has:

$$\mathbf{q}_l^{n+1} = \mathbf{T}_{cell}\mathbf{q}_l^n. \tag{14}$$

By applying Bloch-Floquet periodic boundary condition to the HR-duct periodic system and simplifying an eigenproblem is obtained as:

$$\mathbf{T}_{cell}\mathbf{q} = \mathrm{e}^{\mu}\mathbf{q}, \tag{15}$$

where e^{μ} are the eigenvalues, $\mathbf{q}$ are the eigenvectors, and $\mu = -jkL_{cell}$ is the attenuation constant. From this eigenvalue/eigenvector problem it can be obtained the Bloch wavenumber and the corresponding Bloch wave mode-shapes.

3.1 Transmission Loss (TL) and Forced Response (FRF)

From the unit-cell transfer matrix (Eq. 11), it is possible to calculate the transmission loss (TL) along the duct [7] by:

$$TL = 20log_{10}\left|\frac{A_c + \frac{Sd}{c}B_c + \frac{c}{Sd}C_c + D_c}{2}\right|, \tag{16}$$

and the forced response (FRF) as [11]:

$$\frac{p_l}{U_0} = \frac{Z_{HR}}{A_c + B_c Z_{HR}}. \tag{17}$$

4 Numerical results

Numerical simulations of the HR-duct acoustic periodic system are performed using a TM code implemented in MATLAB environment, and verified for some examples by FE calculated with COMSOL Multiphysics commercial software. For all simulated results, the HR-duct geometry and the air properties are as shown in the Table 1. The cavity area of the HR is given by the difference between the total area HxW and the neck area of the HR.

Table 1. Numerical model geomery and property.

Geometry/Property	Value
Main duct height H_d	0.2 m
Neck width w_n	0.04 m
Neck length L_n	0.48 m
Side branch length H	0.2 m
Side branch height W	0.2 m
Air mass density ρ	1.2 kg/m^3
Air wave velocity c	343 m/s

4.1 Transmission Loss (TL)

Figure 3 compares the transmission loss curves calculated for a unit-cell HR-duct system with the Equivalent-HR calculated by TM (MATLAB) and FE (COMSOL), and also with the Coiling-HR calculated by FE (COMSOL). The results are calculated for a frequency band of DC-150 Hz with a discretization of 0.1 Hz. For the TLs

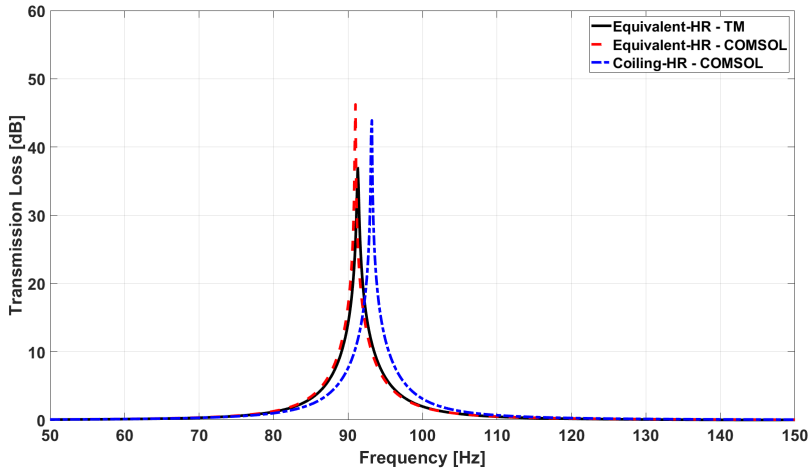

Figure 3. Comparison between TLs calculated TM and FE using Equivalent-HR and Coiling-HR models.

obtained with the Equivalent-HR it can be seen a good agreement between the results calculated by TM and FE, with a TL peak around 91.0 Hz. For the Coiling-HR, the TL peak is shifted by 2.0 Hz (93.0 Hz) above that of Equivalent-HR, showing a relative error of 3%. The wavelength is at least 19x longer than the length of the tube, as shown by Wang et al. [2].

The differences between the Equivalent-HR and the Coiling-HR models are related to the tube winding inside the cavity, as this geometry is not taken into account in the Equivalent-HR calculated by TM and FE. Also, there are differences in amplitudes, which comes from the difference between the methods, since that in FE (COMSOL) all types of waves are being considered, while in TM (MATLAB) only plane waves are considered.

4.2 Dispersion diagram

Figure 4 shows a comparison between the dispersion diagrams calculated with Equivalent-HR model by TM (MATLAB) and FE (COMSOL) with Equivalent- and Coiling-HR models. Note that the real part of

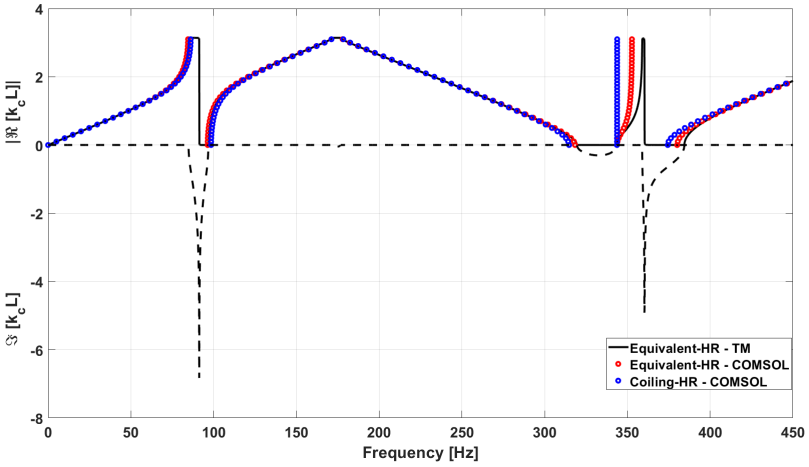

Figure 4. Dispersion diagram for a unit cell

non-dimensional Bloch wavenumber ($\Re\{k_c L_{cell}\}$) are the propagating wave, while the imaginary part of non-dimensional Bloch wavenumbrer ($\Im\{k_c L_{cell}\}$) are the non-propagating waves (evanescent). Also, the FE (COMSOL) calculates only the real part of Bloch wavenumber, which as compared with the TM results in a good agreement between all models. Two different types of bandgaps can be observed: the first type is located in the frequency band close to 91 and 360 Hz, where the sound attenuation occurs due to the local resonance effect provided by the HR. Note that the real part of non-dimensional Bloch wavenumber reaches a constant value of π value (Bragg limit), then at the HR resonance frequency it drops abruptly for a constant value of zero. At the same frequency band the corresponding negative imaginary part of Bloch wavenumber becomes different of zero with a peak at the HR resonance frequency. The second type of bandgaps are located in the frequency bands of 170-180 Hz and 320-340 Hz and are due to Bragg scattering effect generated by periodicity.

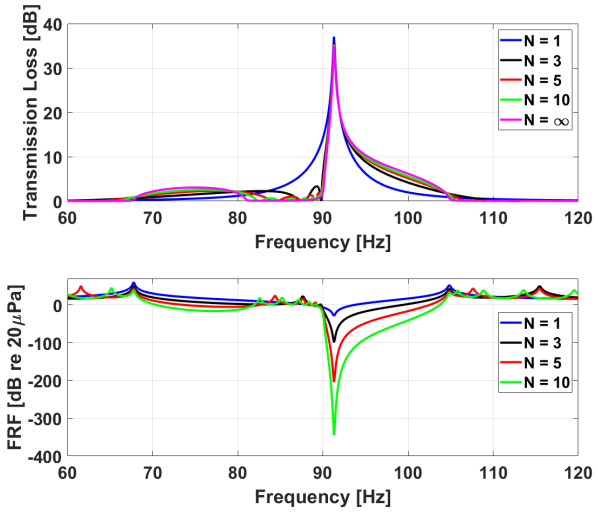

Figure 5. Average $\bar{TL}$ (*top plot*) and FRF (*bottom plot*) calculate by TM for Coiling-HR metamaterial with $N = 1, 3, 5, 10$ cells.

4.3 Sound attenuation for periodic coiling-HR

In this section, the acoustic attenuation of a metamaterial using periodic coiling HR is evaluated for $N = 1, 3, 5, 10$ cells. Figure 5 shows the average $\bar{TL} = TL/N$ (*top plot*) and FRFs (*bottom plot*) calculate by TM. As proposed by [12] the TL for infinite periodic HR cells ($TL_{\inf} = 20log_{10}(\|e^{\mu}\|)$) is also presented. The results demonstrate that as the number of cells increases the $\bar{TL}$ above the HR resonance frequency increases, but bellow it decreases. In the frequency range of 81-89 Hz, unlike $N = 1$ cell that provides an attenuation of 1-9 dB, plane waves propagate without any decay through the periodic resonators when $N = \infty$. However, in the frequency range of 67-81 Hz and 92-104 Hz, as the number of resonators is increased, more noise attenuation is provided.

By considering a unitary volume velocity at the main duct input as the excitation, the acoustic pressure response at the main duct output is obtained for $N = 1, 3, 5, 10$ unit-cells. The results demonstrate that as the number of unit cells increases, the acoustic attenuation around the HR resonance frequency increases.

5 Conclusions

The use of space-coiled resonators brings advantages in dimensional terms compared to Helmholtz resonators, such as the use of small dimensions to attenuate noise with a long wavelength. To increase the range of noise attenuation in a duct, HR were arranged periodically. Through the dispersion diagram it is observed two types of bandgaps caused by the resonant frequency and the periodicity. As the number of resonators increases, more noise attenuation is provided to the system in the frequency bands of 67-81 and 92-104 Hz bands.

Acknowledgements. The authors gratefully acknowledge for the support of the Brazilian funding agencies CAPES (Finance Code 001), CNPq (Grant Reference Numbers 313620/2018 and 151311/2020-0), FAPEMA (Grant Reference Numbers 02294/20, 00857/19, 02730/19, 00824/20 and 00133/21) and FAPESP (Grant Reference Number 2018/15894-0).

Authorship statement. The authors hereby confirm that they are the sole liable persons responsible for the authorship of this work, and that all material that has been herein included as part of the present paper is either the property (and authorship) of the authors, or has the permission of the owners to be included here.

References

[1] R. F. Barron. *Industrial noise control and acoustics*. Marcel Dekker, 2003.
[2] X. Wang, Y. Zhou, J. Sang, and W. Zhu. A generalized model for space-coiling resonators. *Applied Acoustics*, vol. 158, pp. 1–6, 2020.
[3] A. Khettabi, D. Bria, and M. Elmalki. New approach applied to analyzing a periodic helmholtz resonator. *Journal of Materials and Environmental Sciences*, vol. 8, n. 3, pp. 816–824, 2017.
[4] A. Benouhiba, P. Rougeot, N. Andreff, K. Rabenorosoa, and M. Ouisse. Origami-based auxetic tunable helmholtz resonator for noise control. *Smart Materials and Structures*, vol. 30, pp. 1–26, 2021.
[5] A. Selamet and I. Lee. Helmholtz resonator with extended neck. *The Journal of the Acoustical Society of America*, vol. 113, n. 4, pp. 1975–1985, 2003.
[6] X. Shi and C. M. Mak. Helmholtz resonator with a spiral neck. *Applied Acoustics*, vol. 99, pp. 68–71, 2015.
[7] B. V. L. Campos. Controle de ruíduo em dutos usando metamateriais do tipo ressonadores de helmholtz. Master's thesis, University of Campinas, Campinas, 2018.
[8] M. L. Munjal. *Acoustics of Ducts and Mufflers*. John Wiley and Sons, 2014.
[9] A. Selamet and Z. Ji. Circular asymmetric helmholtz resonators. *The Journal of the Acoustical Society of America*, vol. 107, n. 5, pp. 2360–2369, 2000.
[10] Z. Ji. Acoustic length correction of closed cylindrical side-branched tube. *Journal of Sound and Vibration*, vol. 283, pp. 1180–1186, 2005.
[11] S. Singh, C. H. Hansen, and C. Q. Howard. A detailed tutorial for evaluating in-duct net acoustic power transmission in a circular duct with an attached cylindrical helmholtz resonator using transfer matrix method. *Acoustics and Sustainability*, vol. , pp. 1–9, 2008.
[12] X. Wang and C. M. Mak. Wave propagation in a duct with a periodic helmholtz resonators array. *The Journal of the Acoustical Society of America*, vol. 131, n. 2, pp. 1172–1182, 2012.